

Article

Surfactant Intercalation in Li-Al-Based Binary and Ternary Layered Double Hydroxides by the Microwave-Assisted Rapid Ion-Exchange Process and Its Application in Iodine Adsorption

Dileep Kumar Yadav, Sitharaman Uma and Rajamani Nagarajan * 

Materials Chemistry Group, Department of Chemistry, University of Delhi, Delhi 110007, India

* Correspondence: rnagarajan@chemistry.du.ac.in

Abstract: Recognizing the extreme speeds of reactions with microwaves, anionic forms of surfactants (sodium dodecyl sulfate (SDS) and sodium dodecylbenzenesulfonate (SDBS)) have been intercalated successfully by ion-exchange reactions in binary Li-Al and ternary Li-M-Al (M = Mg, Co, Ni, Cu, and Zn) layered double hydroxide (LDH) systems with the aid of microwaves. The samples have been characterized extensively. The basal spacings of 28.2 and 30.4 Å have been estimated for Li-Al-DS and Li-Al-DBS LDH samples, respectively, suggesting a perpendicular arrangement of DS⁻ and DBS⁻ anions in the interlayer space. The characteristic vibration bands of both LDH and the surfactant (DS⁻ and DBS⁻) in the FTIR spectra confirmed the binding mode of surfactant molecules within the interlayers. DS⁻-intercalated Li-Al LDH showed lower thermal stability than the DBS⁻-intercalated sample. The nitrate-intercalated Li-M-Al (M = Mg, Co, Ni, Cu, and Zn) LDHs were ion-exchanged with SDS and SDBS to yield DS⁻- and DBS⁻-intercalated systems. The expanded basal spacings and a change in crystallite morphology confirmed the vertical intercalation of DS⁻ and DBS⁻ in Li-M-Al LDHs. ICP-AES and elemental analyses determined the metal contents and the surfactant content. FTIR spectra of intercalated samples confirmed the surfactant's presence in the interlayer. The presence of Co, Ni, and Cu in Li-M-Al LDHs has been confirmed from UV-visible spectra. The Li-Al-DBS sample adsorbed iodine efficiently from methanol solutions, and the Langmuir model could explain the adsorption data in a better way. The adsorption followed pseudo-second-order kinetics.

Keywords: layered double hydroxides; microwave synthesis; ion-exchange process; surfactant intercalation; iodine adsorption



Citation: Yadav, D.K.; Uma, S.; Nagarajan, R. Surfactant Intercalation in Li-Al-Based Binary and Ternary Layered Double Hydroxides by the Microwave-Assisted Rapid Ion-Exchange Process and Its Application in Iodine Adsorption. *Minerals* **2023**, *13*, 303. <https://doi.org/10.3390/min13030303>

Received: 29 December 2022

Revised: 22 January 2023

Accepted: 20 February 2023

Published: 21 February 2023



Copyright: © 2023 by the authors. Licensee MDPI, Basel, Switzerland. This article is an open access article distributed under the terms and conditions of the Creative Commons Attribution (CC BY) license (<https://creativecommons.org/licenses/by/4.0/>).

1. Introduction

Layered double hydroxides (LDHs) are two-dimensional lamellar inorganic materials. Scientists have researched them actively due to their unique and flexible crystal structures, fascinating physical properties, and versatile applications [1–3]. LDHs can be described by the general formula $[M^{\text{II}}_{1-x-y-z}M^{\text{III}}_xM^{\text{IV}}_yM^{\text{I}}_z(\text{OH})_2](A^{n-})_{(x+2y-z)/n} \cdot m\text{H}_2\text{O}$, where M^{I} , M^{II} , M^{III} , and M^{IV} represent the mono-, di-, tri-, and tetravalent metal cations, respectively; x , y , and z are the mole numbers of M^{III} , M^{IV} , and M^{I} , respectively, per formula unit of the compound; A^{n-} is the interlayer anion of n charge; and m is the molar amount of interlayer water molecules [4,5]. A distinct class of LDHs (Li-Al LDH) is obtained when $y = 0$, $x = 2/3$, and $z = 1/3$, yielding the formula $[M^{\text{I}}_{1/3}M^{\text{III}}_{2/3}(\text{OH})_2](A^{n-})_{1/n} \cdot m\text{H}_2\text{O}$, where A^{n-} may be OH^- , Cl^- , Br^- , NO_3^- , CO_3^{2-} , SO_4^{2-} , and so on. Li-Al LDHs can also be described by the general formula $\text{Li}_x\text{Al}_2(\text{OH})_6(A^{n-})_{x/n} \cdot y\text{H}_2\text{O}$ ($x \leq 1$) considering octahedral vacancies in the metal hydroxide layer [4–7].

The intercalation of a large organic moiety, such as a surfactant, into the interlayer space of LDHs can modify its surface character from hydrophilic to hydrophobic resulting in an enhanced sorption capacity for hydrophobic organic pollutants, a worldwide

problem involving a risk to the wellness of human beings and other habitats by entering the food cycle [8–11]. Surfactants such as sodium dodecyl sulfate (SDS) and sodium dodecylbenzenesulfonate (SDBS) have been widely used where their anions DS^- and DBS^- have been intercalated into LDHs for enhanced sorption of organic contaminants [12–17]. Moreover, the modification of LDHs with surfactants has been a successful strategy for delamination [18–24], having wide applications in different areas of research, such as the preparation of functional coating and membranes [25,26], emulsion stabilizers [27,28], and the measurement of electrophoretic mobility [29].

Anionic-surfactant-intercalated M^{II} -Al LDHs are widely investigated in the literature, but corresponding Li-Al LDHs still need to be well studied. To the best of our knowledge, there are only a few reports on surfactant-intercalated binary Li-Al LDHs [22,30,31], but they need more detailed characterizations, while reports on surfactant-intercalated ternary LDHs are absent. Reports on surfactant-intercalated ternary Li-M-Al LDHs must be available in the literature.

Generally, organo-LDHs are synthesized by the co-precipitation method [13,15–17]. Microwave-assisted reactions have been reported as one of the successful methods for the intercalation of organic anions in LDHs, resulting in hybrid (organic–inorganic) solids [32–34]. Our group successfully reported the microwave-assisted intercalation of inorganic (OH^- , NO_3^- , Cl^-) as well as organic anions obtained from organic acids ($HOOC(CH_2)_nCOOH$ ($n = 0$ to 8)) in Li-Al LDH [35]. Encouraged by the successful intercalation of large molecular organic acids using $LiAlH_4$ as a single-source precursor, we attempted to examine two different structured anionic surfactants' (dodecyl sulfate and dodecylbenzenesulfonate) intercalation by the microwave-assisted ion-exchange method in $[LiAl_2(OH)_6]OH \cdot 2H_2O$ containing OH^- as an interlayer anion. Taking advantage of the synthesis and detailed characterization of nitrate-intercalated ternary LDHs reported by our group recently [36], we have also synthesized surfactant-intercalated ternary Li-M-Al ($M = Mg, Co, Ni, Cu,$ and Zn) LDHs by the ion-exchange method assisted by microwaves.

Radioactive iodine isotope is one of the hazardous, radioactive radionuclides generated as radioactive wastes during the nuclear fuel cycle and has been of great concern to the public [37–39]. The effective removal of radioactive iodine is highly desirable but has remained a significant challenge. The solid adsorption method for capturing radioactive iodine has many advantages, such as high efficiency, simple operation, and low cost [40,41]. Functionalized layered double hydroxides have been reported as excellent adsorbents for the removal of molecular iodine [42–44]. The present report demonstrates Li-Al-DBS LDH as an adsorbent for removing iodine solution in methanol and the results from the kinetics studies.

2. Materials and Methods

2.1. Synthesis

$[LiAl_2(OH)_6]OH \cdot 2H_2O$ was prepared by the procedure reported earlier by our group [35]. Surfactant-intercalated binary Li-Al LDHs (Li-Al-DS and Li-Al-DBS) were prepared using an ion-exchange method by dissolving 91.2 mg (0.32 mmol) of sodium dodecyl sulfate (SDS) (Sigma Aldrich, St. Louis, MO, USA, 99%) and 93.0 mg (0.27 mmol) of sodium dodecylbenzenesulfonate (SDBS) (Sigma Aldrich, St. Louis, MO, USA, 99%), respectively, in 10 mL of H_2O in a 30 mL quartz reactor. Then, 50.5 mg (0.25 mmol) of $[LiAl_2(OH)_6]OH \cdot 2H_2O$ (freshly prepared) was added and subjected to microwave irradiation (Monowave 300, Anton Paar, Graz, Austria). The pH of the reaction mixtures was in the range of 5.1–6.5. The mixture was irradiated for 10 min at 150 °C with varying power in the range of 100–800 W, maintaining the temperature throughout the reaction. Finally, the reaction mixture was cooled to room temperature. The obtained solid products were washed 3–4 times with double-distilled water and 2–3 times with absolute ethanol to remove all the unreacted surfactants. The obtained solids were dried at 60 °C in a hot air oven.

DS^- and DBS^- -anion-intercalated ternary Li-M-Al ($M = Mg, Co, Ni, Cu,$ and Zn) LDHs were synthesized by the ion-exchange reaction of nitrate-intercalated Li-M-Al

(M = Mg, Co, Ni, Cu, and Zn) LDHs with SDS and SDBS, respectively. Nitrate-intercalated Li-M-Al LDHs were synthesized using a procedure as reported earlier [36]. The reaction mixture's pH before irradiation was in the range of 5.5–6.5. The mixture was irradiated for 12–15 min at 150 °C with varied microwave power between 100 and 800 W and, finally, the vessel was cooled to room temperature. The obtained solids were washed 3–4 times with double-distilled water and dried at 60 °C in a hot air oven. In a typical synthesis of surfactant-intercalated Li-M-Al (M = Mg, Co, Ni, Cu, and Zn) LDHs, 45 mg (0.17 mmol) of the LDH was suspended in an aqueous solution containing 63.3 mg (0.22 mmol) of SDS and 66.5 mg (0.19 mmol) of SDBS, respectively, in a 30 mL quartz reactor. The pH of the reaction mixtures varied between 6.1 and 7.5. The mixture was kept under microwave irradiation for 10 min at 150 °C, and microwave power was varied from 100 to 800 W, maintaining the temperature of the reaction mixture. Finally, it was cooled to room temperature. The products were washed 3–4 times with double-distilled water along with 2–3 times with absolute ethanol and placed in a hot air oven at 60 °C for drying.

2.2. Characterization

Powder X-ray diffraction (PXRD) measurements were conducted in a Bragg–Brentano configuration using a Rigaku Mini Flex 600 diffractometer (Rigaku, Osaka, Japan) equipped with a Xe proportional detector employing Cu-K α radiation ($\lambda = 1.5418 \text{ \AA}$). The powders were filled in the mold of the sample holder by sprinkling the sample and were not pressed with a glass slide to avoid any preferred orientation effect. The data were collected over the 2θ range of 5–50° with a scan step size of 0.01° and a scan rate of 3 °/min at room temperature. The metal content analysis was conducted by the inductively coupled plasma atomic emission spectroscopy (ICP-AES) on an ARCOS, simultaneous ICP Spectrometer instrument (SPECTRO Analytical Instruments GmbH, Kleve, Germany) using solutions obtained by dissolving the LDH samples in dilute HCl at 80 °C. The C, H, N, and S contents of the LDH samples were determined using an Elementar Analysensysteme GmbH Vario EL V3.00 elemental analyzer (Elemental Analysensysteme GmbH, Langensfeld, Germany). Fourier transform infrared (FTIR) spectra were gathered using a Perkin Elmer 2000 Fourier transform infrared spectrometer (Perkin Elmer, Waltham, MA, USA) in the spectral range of 400–4000 cm^{-1} using a resolution of 4 cm^{-1} and 64 scans. The powder samples were mixed with KBr in a 1:20 weight ratio and pressed into pellets for recording FTIR spectra. Solid samples' diffuse reflectance spectra (DRS) were measured over the 200–800 nm spectral range using a Perkin-Elmer Lambda 35 scanning double-beam spectrometer (Perkin Elmer, Waltham, MA, USA) with a 50 mm integrating sphere using BaSO₄ as the reference. The thermogravimetric (TG) and differential scanning calorimetry (DSC) experiments were conducted using a NETZSCH STA 449F3 instrument (NETZSCH STA 449F3, Selb, Germany) with a heating rate of 10 °C min^{-1} over 30–800 °C under a flowing N₂ atmosphere. The samples' surface morphology and elemental analysis were probed using a JEOL 6610 LV microscope (JEOL Ltd., Tokyo, Japan) equipped with an energy-dispersive spectrometer (EDS) operating at 20 kV.

2.3. Iodine Adsorption Experiment Details

Different concentrations of stock solutions were prepared by dissolving naturally occurring non-radioactive iodine (I₂) in methanol. The batch method was selected to study the adsorption characteristics. A fixed amount of adsorbent and an iodine solution with the required concentrations were added to the glass beaker. The mixture was stirred for specified time intervals (60–300 min) under dark conditions at room temperature. The solid–liquid separation was performed using centrifugation. The residual concentration of iodine in the supernatant solution was estimated using a UV-visible spectrophotometer (Shimadzu UV-1601, Shimadzu, Kyoto, Japan). The supernatant solution and the adsorbent (if any) were added back to the reaction mixture to avoid mass imbalance and to maintain the reaction equilibrium after taking aliquots to record UV-visible spectra.

The effect of adsorbent dosage was determined using a fixed iodine concentration (25.4 mg/L) and varying the adsorbent amount between 0.8 and 4.1 g/L at room temperature.

Another set of experiments was performed to establish adsorption isotherms, for which a fixed amount of adsorbent (50 mg) was dispersed in a 30 mL iodine solution with differing concentrations (25.4–203.0 mg/L) in the dark at room temperature. The adsorbed iodine amount, at equilibrium (q_e (mg/g)), was estimated using the following expression:

$$q_e = \frac{(C_0 - C_e)}{m} \times V \quad (1)$$

C_0 and C_e are the initial and equilibrium iodine concentrations, m is the mass of the adsorbent, and V is the volume of the solution (in L).

Kinetics studies were conducted by dispersing 50 mg of adsorbent in 101.5 mg/L iodine solution. The suspension was taken out at fixed time intervals, and the absorbance of the supernatant solution was measured using a UV-visible spectrophotometer after centrifugation. The adsorbed iodine amount by the adsorbent at specified time intervals (q_t (mg/g)) is calculated using the expression:

$$q_t = \frac{(C_0 - C_t)}{m} \times V \quad (2)$$

C_0 and C_t are the initial and final iodine concentration after a time interval of t , m is the mass of the adsorbent, and V is the volume of the solution (in L).

3. Results and Discussion

3.1. Surfactant-Intercalated Binary Li-Al LDHs (Li-Al-DS and Li-Al-DBS)

The PXRD pattern of $[\text{LiAl}_2(\text{OH})_6]\text{OH}\cdot 2\text{H}_2\text{O}$ is compared with the products from the reaction of SDS and SDBS with $[\text{LiAl}_2(\text{OH})_6]\text{OH}\cdot 2\text{H}_2\text{O}$ assisted by microwaves in Figure 1. The PXRD pattern of $[\text{LiAl}_2(\text{OH})_6]\text{OH}\cdot 2\text{H}_2\text{O}$ shows typical reflections of LDH indexable in S. G. $C2/m$ reported in the literature [6,35]. The LDH exhibits well-developed (00 l) diffraction peaks corresponding to the basal spacing of 7.55 Å. The PXRD patterns of the LDHs modified with SDS and SDBS show well-ordered (00 l) reflection peaks and shifted to the lower 2θ angles. The patterns can be indexed in the $R\bar{3}m$ space group and agree well with the earlier reported results [22,24,30]. In the PXRD patterns of Li-Al-DS and Li-Al-DBS LDH samples, the characteristic intense basal peak (003) hkl plane along with higher-order peaks such as (006), (009), (0012), (0015), (0018), and (0024) are present, suggesting coherence in all directions with respect to X-ray scattering. The dominance of the PXRD patterns by (00 l) reflections confirms a high crystalline order and well-developed layered structure oriented along the c -axis. The d spacing of basal reflection represented by the (003) plane has been calculated using the expression

$$d_{\text{spacing}} = d_{\text{layer}} + d_{\text{inter}} \quad (3)$$

where d_{layer} represents the thickness of the metal hydroxide layer of the LDH sheet and d_{inter} is the length of the intercalated species and water in the interlayer gallery. The basal spacings of 28.2 and 30.4 Å have been estimated for Li-Al-DS and Li-Al-DBS LDH samples, respectively. The difference in carbon chain length between DS^- (18.3 Å) and DBS^- (21.4 Å) anions can be the cause for the different basal spacings [13,45]. The change in basal spacings from 7.55 Å in $[\text{LiAl}_2(\text{OH})_6]\text{OH}\cdot 2\text{H}_2\text{O}$ to 28.2 and 30.4 Å in Li-Al-DS and Li-Al-DBS LDHs confirmed a successful ion-exchange of OH^- by DS^- and DBS^- anions.

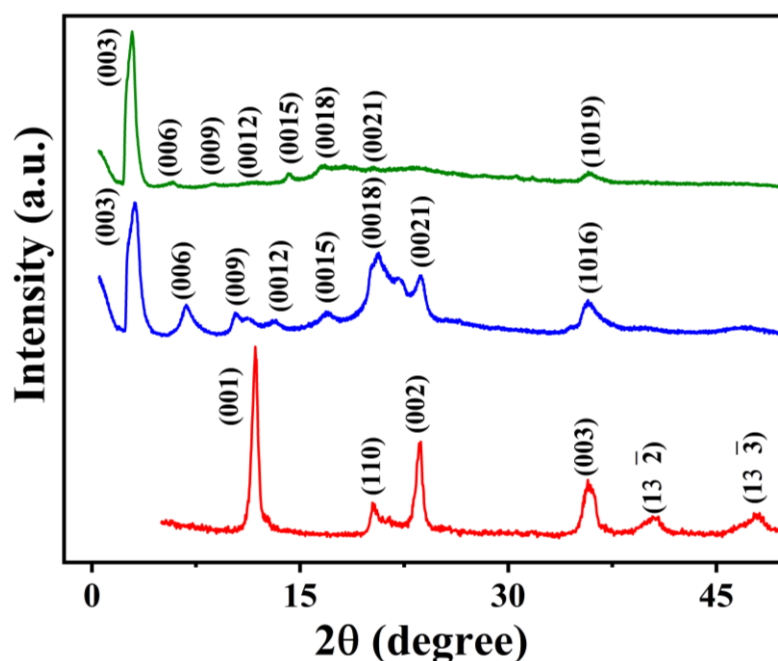


Figure 1. Powder XRD patterns of pristine LDH ($[\text{LiAl}_2(\text{OH})_6]\text{OH}\cdot 2\text{H}_2\text{O}$) (data in red), Li-Al-DS LDH (data in blue), and Li-Al-DBS LDH (data in olive green).

Considering the layer thickness of Li-Al LDH to be 4.8 \AA , the shift around $3\text{--}5 \text{ \AA}$ can be due to the water molecules' presence between DS^- or DBS^- anions in the LDH layer. These results indicate that DS^- and DBS^- anions' molecular chain is arranged in a perpendicular fashion to the LDH layers or parallel to the c axis in the interlayer space [22,24,30]. Considering the layer charge density of the layers, the area required for the anionic surfactant molecules, and the gain in the van der Waals energy after the close packing of the alkyl chains in the layers, it is suggested that the structure of DS^- and DBS^- in the interlayer space is a perpendicular monolayer structure, not with a tilted bilayer structure [17].

The metal contents of Li-Al-DS and Li-Al-DBS LDH samples, derived from the ICP-AES measurements, are shown in Table 1. Li and Al are present in these samples, with Al: Li nominal ratios of 2.15 and 2.06 in DS^- - and DBS^- -intercalated Li-Al LDHs.

Table 1. The elemental content of surfactant (DS^- and DBS^-)-intercalated Li-Al and Li-M-Al ($M = \text{Mg}, \text{Co}, \text{Ni}, \text{Cu}, \text{and Zn}$) LDH from ICP-AES measurement.

LDHs	Content of Elements (mol %)							
	Li	Al	Mg	Co	Ni	Cu	Zn	Cd
Li-Al-DS	9.2	19.8	-	-	-	-	-	-
Li-Mg-Al-DS	2.4	17.1	6.1	-	-	-	-	-
Li-Co-Al-DS	1.8	16.1	-	9.3	-	-	-	-
Li-Ni-Al-DS	2.1	17.1	-	-	7.3	-	-	-
Li-Cu-Al-DS	1.7	16.9	-	-	-	8.7	-	-
Li-Zn-Al-DS	2.0	17.6	-	-	-	-	7.2	-
Li-Al-DBS	9.5	19.6	-	-	-	-	-	-
Li-Mg-Al-DBS	2.2	17.5	6.5	-	-	-	-	-
Li-Co-Al-DBS	1.9	16.9	-	8.6	-	-	-	-
Li-Ni-Al-DBS	1.9	17.1	-	-	7.4	-	-	-
Li-Cu-Al-DBS	1.8	16.4	-	-	-	9.1	-	-
Li-Zn-Al-DBS	2.3	17.9	-	-	-	-	6.8	-

C, H, N, and S microanalysis confirms their presence in both the LDH samples establishing the existence of surfactants in the interlayer space of the LDHs (Table S1).

The FTIR spectra of $[\text{LiAl}_2(\text{OH})_6]\text{OH}\cdot 2\text{H}_2\text{O}$, Li-Al-DS, and Li-Al-DBS are shown in Figure 2. The assignment of observed bands is summarized in Table 2. The strong and broad band centered at around 3440, 3455, and 3465 cm^{-1} in OH^- , DS^- , and DBS^- -intercalated Li-Al LDH, respectively, arise from the O-H stretching modes of hydroxyl groups in the brucite-like layers and interlayer water molecules. This band is broadened due to hydrogen bonding. This band shifts from 3440 (observed in $[\text{LiAl}_2(\text{OH})_6]\text{OH}\cdot 2\text{H}_2\text{O}$ LDH) to 3455 and 3465 cm^{-1} in surfactant-intercalated LDH. This is due to the weakening of the hydrogen bonding as a consequence of the decrease in H_2O content. A decrease in intercalated H_2O content is related to the change in the surface property from hydrophilic to hydrophobic due to the intercalation of surfactants in the interlayer space of the parent LDH ($[\text{LiAl}_2(\text{OH})_6]\text{OH}\cdot 2\text{H}_2\text{O}$). Moreover, the electrostatic attraction between the LDH sheet and intercalate decreases when the interlayer anion changes from OH^- to DS^- and DBS^- anions [46,47].

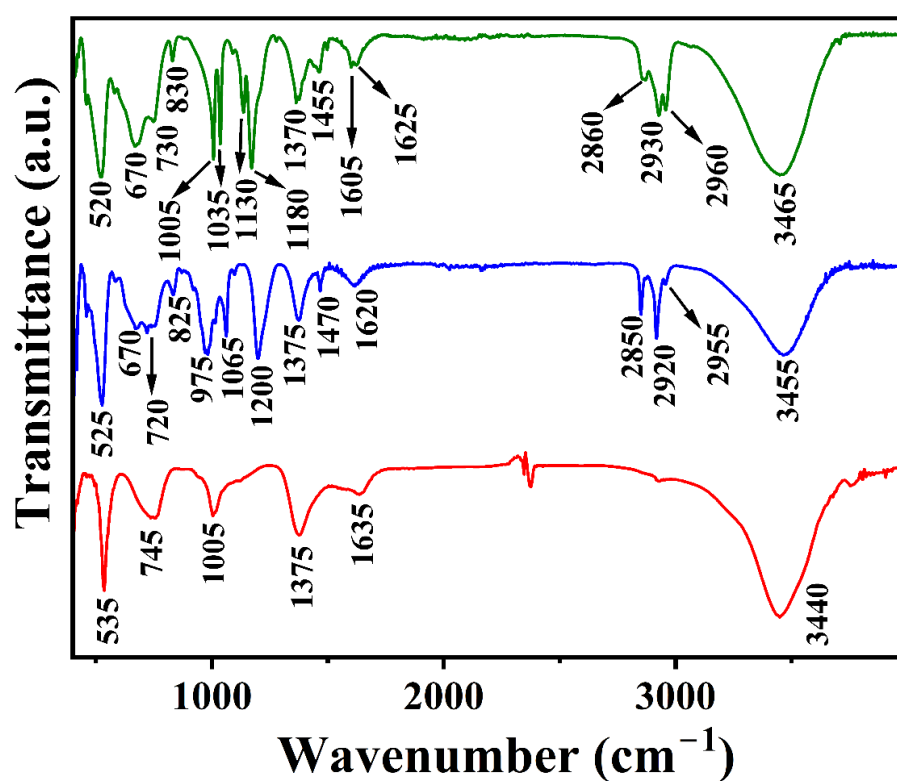


Figure 2. FTIR spectra of pristine LDH ($[\text{LiAl}_2(\text{OH})_6]\text{OH}\cdot 2\text{H}_2\text{O}$) (data in red), Li-Al-DS LDH (data in blue), and Li-Al-DBS LDH (data in olive green).

The O-H bending mode of interlayer and adsorbed water molecules can be seen at 1635, 1620, and 1625 cm^{-1} in OH^- , DS^- , and DBS^- -intercalated Li-Al LDHs, respectively. The weak bands located at 1375 cm^{-1} in $[\text{LiAl}_2(\text{OH})_6]\text{OH}\cdot 2\text{H}_2\text{O}$ and Li-Al-DS LDHs and at 1370 cm^{-1} in Li-Al-DBS LDH correspond to the ν_3 C-O stretching modes of atmospheric CO_3^{2-} in the interlayer space of the LDH [46,48–51].

The absorption band centered at 1005 cm^{-1} in $[\text{LiAl}_2(\text{OH})_6]\text{OH}\cdot 2\text{H}_2\text{O}$ is assigned to the vibration of the hydroxyl groups coordinated to the cations (Li^+ and Al^{3+}) in the octahedral layers [4,7]. The bands at 745 and 535 cm^{-1} arise from the Al-O vibrations [4,7,35].

The two prominent bands at 2920 and 2850 cm^{-1} in Li-Al-DS LDH can be assigned to the $\nu_{\text{C-H}}$ anti-symmetric and symmetric stretching mode for $-\text{CH}_2$. The shoulder at 2960 cm^{-1} corresponds to the $\nu_{\text{C-H}}$ anti-symmetric stretching mode of the terminal $-\text{CH}_3$ group and the band corresponding to C-H bending can be observed at 1470 cm^{-1} . The bands around 1200 and 1065 cm^{-1} are due to the asymmetric and symmetric $\nu_{\text{S=O}}$ stretching vibration of DS^- anions. The asymmetric and symmetric stretching frequency of S=O

shifts to lower wavenumbers than SDS [46,48,49,51]. A downward shift in wavenumber corresponds to a weakening of the S=O bond strength, suggesting the presence of a hydrogen bond between the LDH layer and sulfate groups (S=O ... H-O-Al) in addition to electrostatic attraction and van der Waals forces between LDH layers and surfactant molecules [50,51]. The bands at 975 and 825 cm^{-1} represent the stretching vibration modes of C-O and S-O, respectively. The bands at 720 and 525 cm^{-1} are due to the Al-O stretching mode. The ν_4 bending angular mode of CO_3^{2-} anions manifested at 670 cm^{-1} [51].

Table 2. Assignment of FTIR bands in Li-Al-OH ($[\text{LiAl}_2(\text{OH})_6]\text{OH}\cdot 2\text{H}_2\text{O}$), Li-Al-DS, and Li-Al-DBS LDHs.

LDH	Band Positions (cm^{-1})	Type of Vibrations	References
Li-Al-OH	3440	O-H stretching of interlayer H_2O or M-OH	[4,7,35]
	1635	O-H bending of H_2O	[4,7,35]
	1375	ν_3 C-O stretching mode of CO_3^{2-} anion	[4,7]
	1005	Vibrations of the OH groups in the Li-Al LDH layer	[4,7]
	745, 535	Al-O stretching	[4,7,35]
Li-Al-DS	3455	O-H stretching of interlayer H_2O or M-OH	[46,48–51]
	1620	O-H bending of H_2O	[46,48–51]
	1375	ν_3 C-O stretching mode of CO_3^{2-} anion	[46,48–51]
	2920	C-H anti-symmetric stretching of $-\text{CH}_2$	[46,48,49,51]
	2850	C-H symmetric stretching of $-\text{CH}_2$	[46,48,49,51]
	2955	C-H anti-symmetric stretching of the terminal $-\text{CH}_3$	[46,48,49,51]
	1470	C-H bending	[46,48,49,51]
	1200	S=O anti-symmetric stretching	[46,48,49,51]
	1065	S=O symmetric stretching	[46,48,49,51]
	975	C-O stretching	[46,48,49,51]
	825	S-O stretching	[46,48,49,51]
	720, 525	Al-O stretching	[4,7,35]
670	ν_4 bending angular mode of CO_3^{2-} anion	[51]	
Li-Al-DBS	3465	O-H stretching of interlayer H_2O or M-OH	[46,48–51]
	1625	O-H bending of H_2O	[46,48–51]
	1370	ν_3 C-O stretching mode of CO_3^{2-} anion	[46,48–51]
	2930	C-H anti-symmetric stretching of $-\text{CH}_2$	[48,50,51]
	2860	C-H symmetric stretching of $-\text{CH}_2$	[48,50,51]
	2960	C-H anti-symmetric stretching of the terminal $-\text{CH}_3$	[48,50,51]
	1605	C-C stretching (benzene group)	[48,50,51]
	1470	C-H bending	[48,50,51]
	1455	C=C stretching (benzene group)	[48,50,51]
	1180	S=O anti-symmetric stretching	[48,50,51]
	1035	S=O symmetric stretching	[48,50,51]
	1130, 1005	C-H in plane bending modes (benzene group)	[48,50,51]
	830	S-O stretching	[48,50,51]
	730, 520	Al-O stretching	[4,7,35]
670	ν_4 bending angular mode of CO_3^{2-} anion	[51]	

The FTIR spectrum of the Li-Al-DBS LDH shows the characteristic absorption bands of both LDH and SDBS (Figure 2). The characteristic vibration bands are detected for the SO_3 group (symmetric stretching at 1035 cm^{-1} and anti-symmetric stretching at 1180 cm^{-1}), benzene group (C-C stretching at 1605 cm^{-1} , C-H in-plane bending vibration modes at 1005, 1130, and 830 cm^{-1} , C=C stretching band at 1455 cm^{-1}), and alkyl group asymmetric stretching of CH_3 and CH_2 at 2960 and 2930 cm^{-1} , respectively, and symmetric stretching of CH_3 and CH_2 at 2860 and 2855 cm^{-1} , respectively [45,48,50,51]. The bands located near 520 and 730 cm^{-1} are due to Al-O stretching modes, and the band centered at 670 cm^{-1} is due to ν_4 bending angular modes of CO_3^{2-} anions (Table 2). The presence of CO_3^{2-} absorption bands in the FTIR spectra establishes the co-intercalation of atmospheric CO_3^{2-}

ions (in traces) with surfactants in the interlayer space of the LDHs, and both surfactants and carbonate anions balance the LDH layer charges.

The diffuse reflectance spectra of DS^- - and DBS^- -anion-intercalated Li-Al LDHs are shown in Supplementary Materials Figure S1. The spectra contain peaks at 245 and 265 nm for Li-Al-DS and Li-Al-DBS LDHs, respectively, originating from sulfate and sulfonate groups [52].

The TG-DSC traces of $[\text{LiAl}_2(\text{OH})_6]\text{OH}\cdot 2\text{H}_2\text{O}$, Li-Al-DS, and Li-Al-DBS are shown in Figure 3. The $[\text{LiAl}_2(\text{OH})_6]\text{OH}\cdot 2\text{H}_2\text{O}$ sample demonstrates two-step weight loss in TGA accompanied by one broad endothermic peak in DSC measurement (Figure 3a). The first weight loss step is due to the removal of intercalated water molecules while the second step indicates the decomposition of atmospheric CO_3^{2-} and OH^- anions in the interlayer region along with the de-hydroxylation of the metal hydroxide layer, respectively. This result is consistent with the earlier reports [7,35].

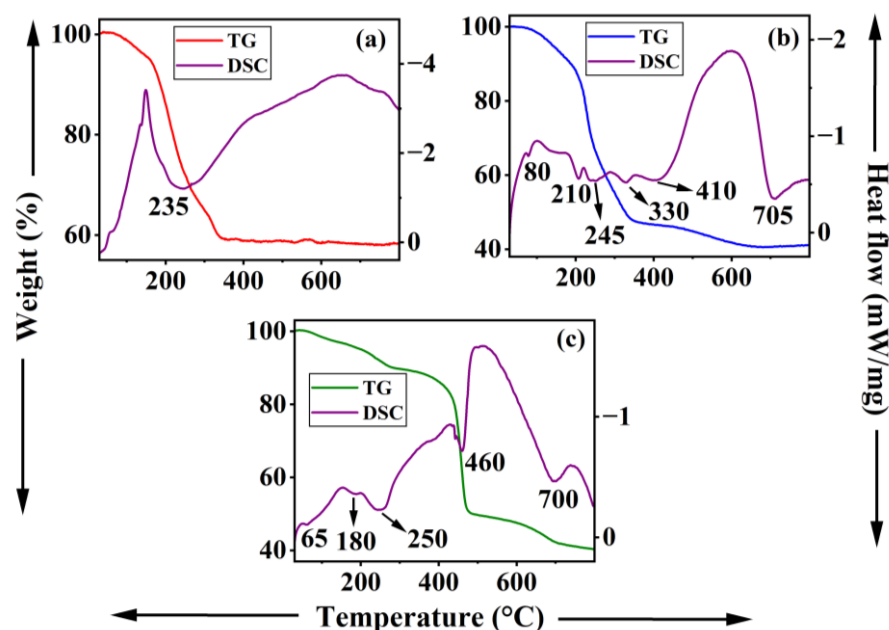


Figure 3. TG-DSC traces of (a) pristine LDH ($[\text{LiAl}_2(\text{OH})_6]\text{OH}\cdot 2\text{H}_2\text{O}$), (b) Li-Al-DS LDH, and (c) Li-Al-DBS LDH.

For the Li-Al-DS sample, the weight loss can be divided into two stages (Figure 3b). The first stage in the temperature range of 30–195 °C, with a weight loss of ~12 wt% and one endothermic peak at 80 °C in the DSC curve, is assigned to the release of physisorbed and interlayer water molecules. The second stage in the temperature range 190–700 °C, with a weight loss of ~48 wt% and four endothermic peaks at ~210, 245, 330, and 410 °C, can be attributed to the decomposition of intercalated DS^- anions along with the loss of atmospheric impurity CO_3^{2-} in the interlayer space and dehydroxylation of brucite-like layers [49,51,53].

The thermal decomposition of the Li-Al-DBS LDH samples also roughly takes place in two stages (Figure 3c). In the first stage, weight loss of ~12 wt% in the temperature range of 30–300 °C, accompanied by a major endothermic peak at ~250 °C, is due to the removal of adsorbed and intercalated water molecules. The second stage, with a weight loss of ~44 wt% in the temperature range of 300–800 °C accompanied by two endothermic peaks at 460 and 700 °C, denotes the decomposition of the alkyl chain and benzene ring of DBS^- anions and the removal of impurity of atmospheric carbonate anions along with the dehydroxylation of brucite-like layers [51,53]. The thermal behavior of intercalated LDH depends on the nature of the surfactants, basically in the second stage of the thermal decomposition process in which the layered structure completely collapses. The thermal decomposition of Li-Al-DBS

LDH stretches to higher temperatures owing to the decomposition of the benzene rings and hydrocarbon chains in the absence of free oxygen [51,53]. DS[−]-intercalated Li-Al LDH shows lower thermal stability than DBS[−]-intercalated LDH (Figure 3b,c).

Significant variations in the weight loss steps and endotherms of Li-Al-DS and Li-Al-DBS LDHs from LiAl₂(OH)₆]OH·2H₂O LDH corroborate well with the modification of the interlayer gallery of Li-Al LDH by the surfactants.

The morphologies and elemental analyses of Li-Al-DS and Li-Al-DBS LDHs are investigated with the help of SEM attached with an EDS (Figure S2). Both samples exhibit lamellar structures, and similar morphological features can be seen irrespective of the type of surfactants. Flaky morphology can be observed in the Li-Al-DS LDH sample (Figure S2a), while the Li-Al-DBS sample is composed of plate-like architectures (Figure S2b). The morphology of both LDH samples possesses more or less sharp edges (Figure S2). Similar morphologies have been seen earlier in other surfactant-intercalated LDHs [49,51,53]. EDS analyses of both surfactant-intercalated Li-Al LDHs confirm the presence of Al, C, S, and O in the sample (Figure S2a,b, Table S2). The EDS analyses also demonstrate a high content of carbon in the DBS[−]-intercalated sample than the DS[−]-intercalated one. This is in good agreement with the greater carbon content in DBS[−] anions than in DS[−] anions.

The chemical compositions of both Li-Al-DS and Li-Al-DBS LDHs, inferred from the ICP-AES and elemental analyses, and considering the presence of surfactants and carbonate anions, are presented in Table 3. The molar content of lithium per formula weight was 0–1 range, agreeing with the general formula of Li-Al LDHs.

Table 3. The chemical composition of Li-Al-DS, Li-M-Al-DS, Li-Al-DBS, and Li-M-Al-DBS LDHs without considering interlayer water molecules.

LDHs	Chemical Composition
Li-Al-DS	Li _{0.92} Al _{1.98} (OH) ₆ (DS) _x (CO ₃) _y
Li-Mg-Al-DS	Li _{0.24} Mg _{0.61} Al _{1.71} (OH) ₆ (DS) _x (CO ₃) _y
Li-Co-Al-DS	Li _{0.18} Co _{0.93} Al _{1.61} (OH) ₆ (DS) _x (CO ₃) _y
Li-Ni-Al-DS	Li _{0.21} Ni _{0.73} Al _{1.71} (OH) ₆ (DS) _x (CO ₃) _y
Li-Cu-Al-DS	Li _{0.17} Cu _{0.87} Al _{1.69} (OH) ₆ (DS) _x (CO ₃) _y
Li-Zn-Al-DS	Li _{0.20} Zn _{0.72} Al _{1.76} (OH) ₆ (DS) _x (CO ₃) _y
Li-Al-DBS	Li _{0.95} Al _{1.96} (OH) ₆ (DBS) _x (CO ₃) _y
Li-Mg-Al-DBS	Li _{0.22} Mg _{0.65} Al _{1.75} (OH) ₆ (DBS) _x (CO ₃) _y
Li-Co-Al-DBS	Li _{0.19} Co _{0.86} Al _{1.69} (OH) ₆ (DBS) _x (CO ₃) _y
Li-Ni-Al-DBS	Li _{0.19} Ni _{0.74} Al _{1.71} (OH) ₆ (DBS) _x (CO ₃) _y
Li-Cu-Al-DBS	Li _{0.18} Cu _{0.91} Al _{1.64} (OH) ₆ (DBS) _x (CO ₃) _y
Li-Zn-Al-DBS	Li _{0.23} Zn _{0.68} Al _{1.79} (OH) ₆ (DBS) _x (CO ₃) _y

3.2. Surfactant-Intercalated Ternary Li-M-Al-LDHs (M = Mg, Co, Ni, Cu, and Zn)

The synthesis of surfactant-intercalated ternary Li-M-Al (M = Mg, Co, Ni, Cu, and Zn) LDHs was attempted by ion-exchange method from their corresponding nitrate-intercalated Li-M-Al LDH [36] using microwave irradiation. Here, we have included the PXRD pattern (Figures 4 and 5), FTIR spectrum (Figure S3a), and TG-DSC traces (Figure S3b) of the parent Li-Mg-Al-NO₃ LDH for comparison. All other parent ternary LDHs exhibit similar PXRD patterns. The PXRD pattern of Li-Mg-Al-NO₃ is dominated by (002) and (004) reflections indexable in *P6₃/m* or *P6₃/mcm* [36]. The basal spacing was 8.92 Å consistent with reported hydrated NO₃[−]-intercalated LDHs [35,36]. The labile NO₃[−] in the interlayer space is easily exchanged by dodecyl sulfate and dodecylbenzenesulfonate anions resulting in surfactant-intercalated ternary Li-M-Al-LDHs as revealed by the PXRD patterns of Li-M-Al-DS and Li-M-Al-DBS (M = Mg, Co, Ni, Cu, and Zn) LDH samples (Figures 4 and 5). There is a clear shift in the diffraction peaks towards the lower 2θ angles from the parent Li-Mg-Al-NO₃ LDH to Li-Al-DS (Figure 4) and Li-Al-DBS (Figure 5) LDHs. All the reflections are indexable in the *R3̄m* space group, confirming the phase purity of the products.

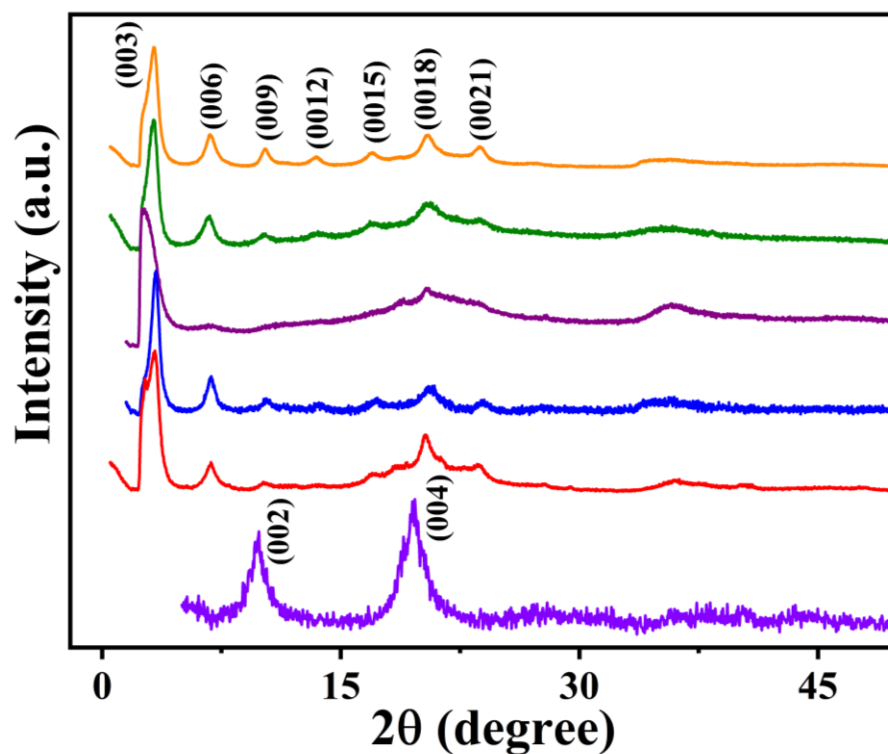


Figure 4. PXRD patterns of Li-Mg-Al-NO₃ LDH (data in violet) and Li-M-Al-DS LDHs (M = Mg (data in red), Co (data in blue), Ni (data in purple), Cu (data in olive green), and Zn (data in orange)).

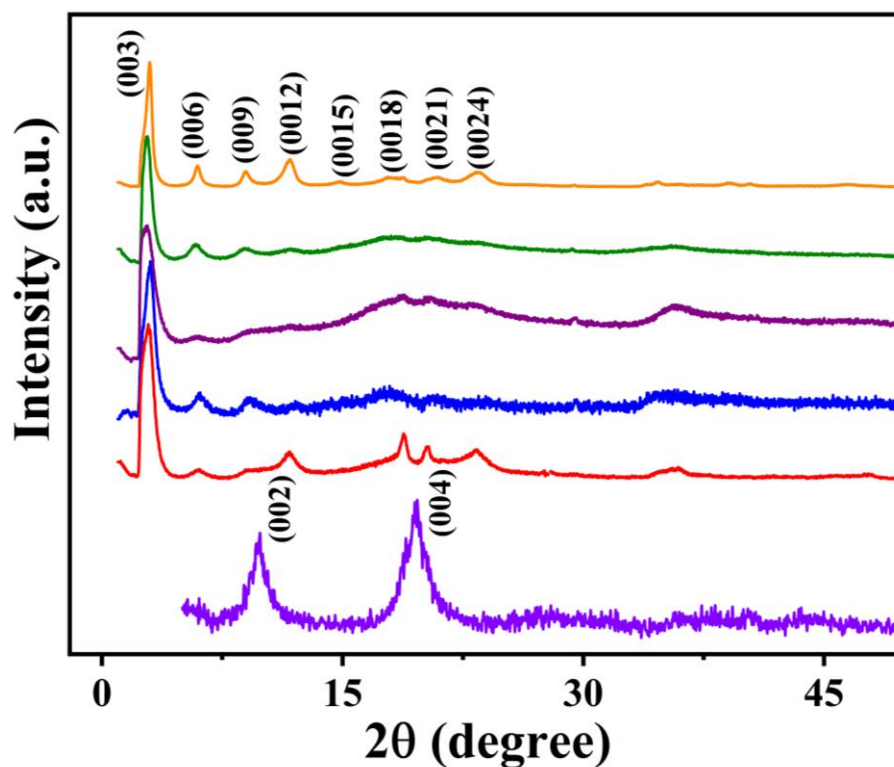


Figure 5. PXRD patterns of Li-Mg-Al-NO₃ LDH (data in violet) and Li-M-Al-DBS LDHs (M = Mg (data in red), Co (data in blue), Ni (data in purple), Cu (data in olive green), and Zn (data in orange)).

The PXRD patterns of both Li-M-Al-DS and Li-M-Al-DBS LDH samples are dominated by reflections of (00*l*) planes, suggesting the successful intercalation of surfactant molecules

(Figures 4 and 5) [22,24,30]. The basal spacings of DS⁻-intercalated Li-M-Al LDHs are 27.0, 26.4, 33.2, 27.2, and 27.4 Å for Mg, Co, Ni, Cu, and Zn incorporated samples, respectively, which confirm the vertical intercalation of DS⁻ in the interlayer space in an anti-parallel arrangement (Figure 4). Similarly, Li-M-Al-DBS LDHs demonstrate basal spacings of 30.1, 29.2, 32.6, 32.0, and 29.8 Å for Mg, Co, Ni, Cu, and Zn incorporated samples, respectively, confirming the successful DBS⁻ anion intercalation in the interlayer gallery (Figure 5). The basal spacings are different for different metal ions in Li-M-Al-DS and Li-M-Al-DBS (M = Mg, Co, Ni, Cu, and Zn) LDHs, respectively. The basal spacing of the LDHs basically depends on the extent, nature, and configuration (molecular size and stereochemistry) of surfactants, the nature of metal ions in the brucite-like layer, the charge density of the brucite-like layer, and the extent of water molecules in the interlayer space [17]. Here, the nature and configuration of DS⁻ and DBS⁻ anions are the same in Li-M-Al-DS (Figure 4) and Li-M-Al-DBS (Figure 5), respectively; therefore, only the layer charge density and nature of the metal ions in the LDH framework determined the basal spacings.

Ni-containing samples in both DS⁻- and DBS⁻-anion-intercalated ternary LDHs exhibit the highest basal spacing, which can be due to a large number of water molecules in the interlayer space along with surfactants. The Ni-containing sample shows the lowest ordering along the *c*-axis, demonstrated by the absence of higher-order (00*l*) reflections owing to the large extent of water molecules or low crystallinity. Li-Zn-Al-DS and Li-Zn-Al-DBS samples show good crystallinity exhibiting multiple (00*l*) reflections that confirm that crystallites are well ordered in the stacking *c*-direction and intercalated DS⁻ and DBS⁻ anions are oriented in an orderly fashion in the interlayer gallery of the LDHs.

The metal content of all the surfactant-intercalated ternary Li-M-Al (M = Mg, Co, Ni, Cu, and Zn) LDHs estimated from ICP-AES analyses are presented in Table 1. All the samples contain lithium, aluminium, and respective divalent metal ions confirming the successful ternary LDHs formation. The elemental ratios were almost similar to the Li-M-Al LDHs before intercalation, ensuring the stability of the LDH samples during ion-exchange reactions [36]. C, H, N, and S analyses of all the ternary Li-M-Al (M = Mg, Co, Ni, Cu, and Zn) LDHs are compiled in Table S1. All the samples show the presence of elements C, H, and S, further confirming surfactant intercalation. Nitrogen's absence confirms the complete exchange of nitrate in ternary Li-M-Al LDHs by surfactants.

The FTIR spectrum of Li-Mg-Al-NO₃ LDH is displayed in Figure S3a. The absorption bands characteristic of O-H stretching and O-H bending are seen at 3440 and 1635 cm⁻¹, respectively. The characteristic band due to the presence of NO₃⁻ is seen at 1380 cm⁻¹. The Al-OH deformation band and vibration of hydroxyl groups coordinated with the Li-Mg-Al layer are observed at 945 and 1020 cm⁻¹, respectively. The bands in the lower wavenumber region 900–400 cm⁻¹ signify the M-O vibrations [4,7,35,36].

FTIR spectra of Li-M-Al-DS (M = Mg, Co, Ni, Cu, and Zn) LDHs show the characteristic bands related to DS⁻ anions and LDHs (Figure 6). The band centered at 3450 cm⁻¹ is due to superimposed O-H stretching vibrations of hydroxyl groups and interlayer water molecules, while the O-H bending vibration of water molecules in the interlayer space is seen at 1620 cm⁻¹. The weak band attributable to the unavoidable impurity of atmospheric carbonate anions can be located at 1375 cm⁻¹. The peaks at 2955, 2920, and 2850 cm⁻¹ can be assigned to asymmetric and symmetric stretching modes CH₃ and -CH₂ in dodecyl sulfate anions. The characteristic bands of the SO₄⁻ group in Li-M-Al-DS LDHs are observed at 1200, 1060, and 825 cm⁻¹. The band due to C-O stretching and C-H bending vibrations are seen at 975 and 1465 cm⁻¹, respectively [46,48,51]. The bands related to M-O-M and O-M-O stretching and bending modes are present in the 800–400 cm⁻¹ range. The increased number of bands in the 800–400 cm⁻¹ regions compared to Li-Al-DS LDH can be attributed to additional vibrations (stretching and bending) of divalent metal (Mg, Co, Ni, Cu, and Zn) ions in the LDH framework.

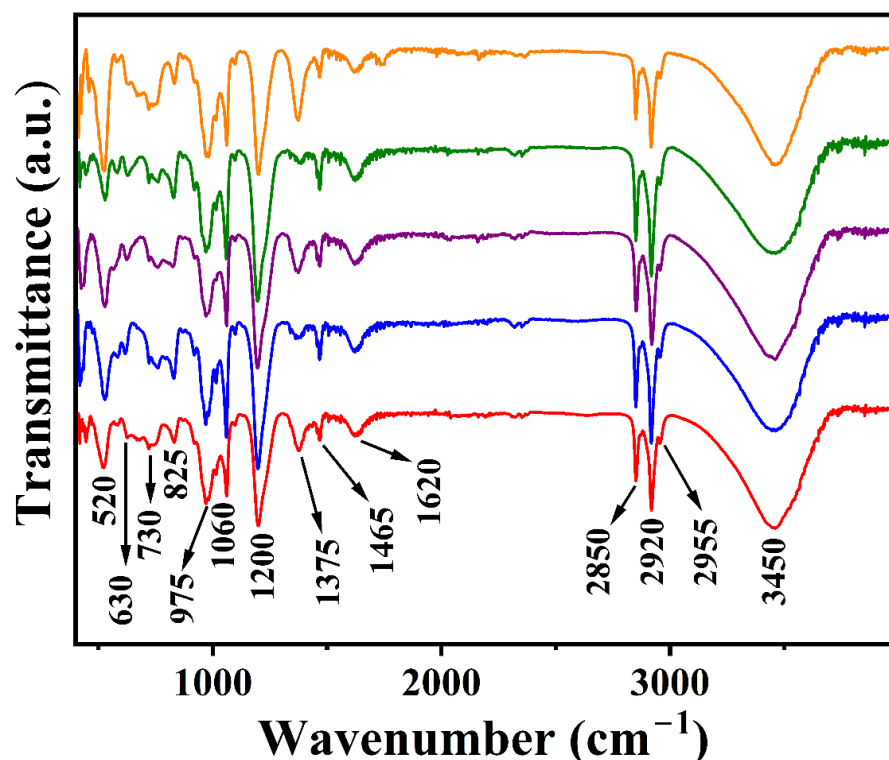


Figure 6. FTIR spectra of Li-M-Al-DS LDHs (M = Mg (data in red), Co (data in blue), Ni (data in purple), Cu (data in olive green), and Zn (data in orange)).

The FTIR spectra of Li-M-Al-DBS LDHs (M = Mg, Co, Ni, Cu, and Zn) are reproduced in Figure 7, from which the existence of DBS^- anions in the interlayer region is established. The characteristic bands related to the O-H stretching mode of overlapping hydroxyl groups in the metal hydroxyl layer and interlayer water molecules are present at 3460 cm^{-1} . The band at 1625 cm^{-1} can be assigned to the O-H bending vibration of intercalated water molecules. The band centered at 1370 cm^{-1} is assigned to impurity carbonate anions. The characteristic vibration bands of the SO_3^- group of DBS^- anions are observed at 1175 and 835 cm^{-1} . The bands that emerged at 1005 and 1460 cm^{-1} can be attributed to the benzene ring in DBS^- anions [46,48,51]. The bands in the region $800\text{--}400\text{ cm}^{-1}$ can be assigned to M-O-M and O-M-O stretching and bending vibrations. The bands arising from DS^- and DBS^- anions, including C-H of the alkyl chain, aromatic C-H, aromatic C=C, and sulfate or sulfonate groups, are evident in the FTIR spectra, substantiating the occurrence of surfactant anions in the LDH interlayer space.

It is not straightforward to distinguish different divalent metal ions incorporated in LDHs based on FTIR spectra. The FTIR spectra of all the ternary LDHs indicate the co-intercalation of carbonate anions in the interlayer space of LDHs and surfactants.

The optical properties of both ternary Li-M-Al-DS and Li-M-Al-DBS (M = Mg, Co, Ni, Cu, and Zn) LDHs are studied by UV-vis DRS measurement (Figure S4a,b). The bands centered at 220 and 260 nm in the UV region of Li-M-Al-DS and Li-M-Al-DBS LDHs confirm successful surfactant intercalation in the interlayer gallery (Figure S4a,b). The Co-containing sample shows characteristic bands at 530 and 650 nm due to electronic transitions ${}^4T_{1g}({}^4F) \rightarrow {}^4T_{1g}({}^4P)$ and ${}^4T_{1g}({}^4F) \rightarrow {}^4A_{2g}({}^4F)$ of Co^{2+} -ion (d^7 , high spin), which is further corroborated by the light pink color of the LDH sample. The light blue color of the Ni-containing sample is substantiated by characteristic bands of Ni^{2+} in the visible region at 420, 650, and 740 nm due to ${}^3A_{2g}({}^3F) \rightarrow {}^3T_{1g}({}^3P)$, ${}^3A_{2g}({}^3F) \rightarrow {}^3T_{1g}({}^3F)$, and the spin-forbidden transition ${}^3A_{2g}({}^3F) \rightarrow {}^1E_g({}^1D)$ of Ni^{2+} ions, respectively. The additional band located at 375 nm can be attributed to ligand-to-metal charge transfer (OH-Ni). The broad band at 700–800 nm in dodecyl-sulfate- and dodecyl-benzenesulfonate-intercalated

Li-Cu-Al LDHs can be assigned to the ${}^2E_g ({}^2D) \rightarrow {}^2T_{2g} ({}^2D)$ electronic transition of Cu^{2+} , which is responsible for the blue color of the samples. Based on the color of the sample and their characteristic bands in the visible region of DRS, transition metal ions (Co, Ni, and Cu) containing LDHs are distinguished.

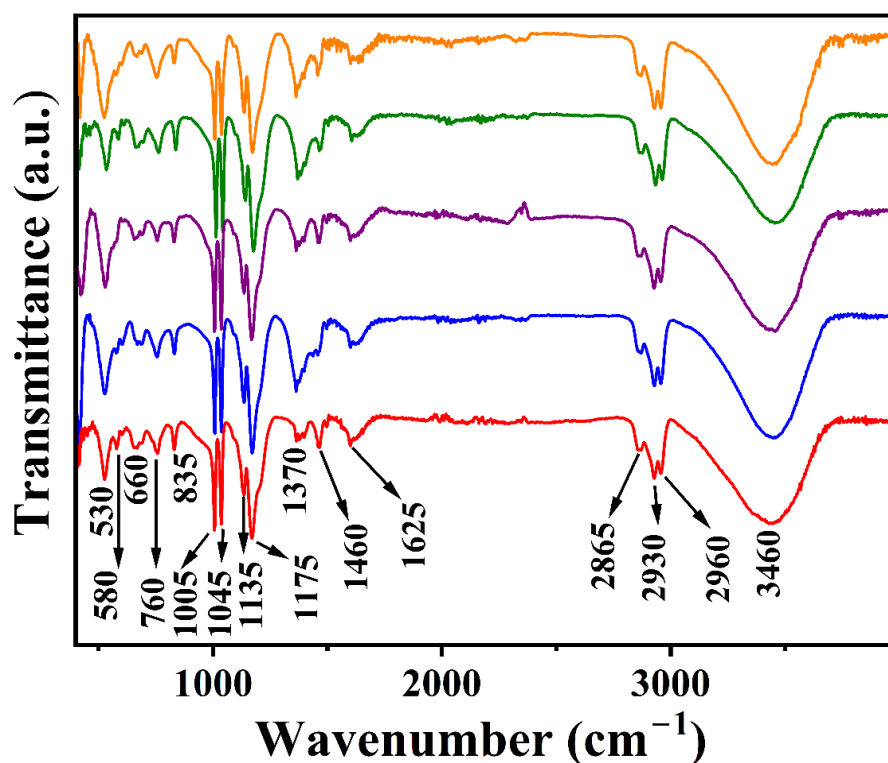


Figure 7. FTIR spectra of Li-M-Al-DBS LDHs (M = Mg (data in red), Co (data in blue), Ni (data in purple), Cu (data in olive green), and Zn (data in orange)).

Figure 8 shows the TG-DSC traces of Li-M-Al-DS (M = Mg, Co, Ni, Cu, and Zn) LDHs. All the samples exhibit characteristic weight loss steps arising from the decomposition of dodecyl sulfate anions in the interlayer gallery. The weight loss below 200 °C can be attributed to the removal of physically adsorbed or intercalated water molecules. The major weight loss in the temperature range of 200–700 °C indicates the decomposition of the alkyl chain of DS^- anions and removal of impurity CO_3^{2-} anions in the interlayer space and removal of hydroxyl groups of metal hydroxide layers. The thermal decomposition of all Li-M-Al-DS LDHs is accompanied by several endothermic peaks in DSC measurement, which confirm that the decomposition of the alkyl chain of DS^- anions took place in many steps [51,53].

TG-DSC curves of DBS^- -intercalated ternary Li-M-Al LDHs are shown in Figure 9. All the samples show major weight loss basically in two temperature regions. The removal of physisorbed and interlayer water molecules occurs below 200 °C. The decomposition of the hydrocarbon chain and benzene ring of DBS anions takes place beyond 200 °C, which overlaps with the removal of impurity carbonate anions and decomposition of the LDH framework. Similar to DS^- -intercalated LDHs, the decomposition of DBS anions is also accompanied by several endothermic peaks in DSC measurement, suggesting a loss of alkyl and benzene moiety in many steps [51,53].

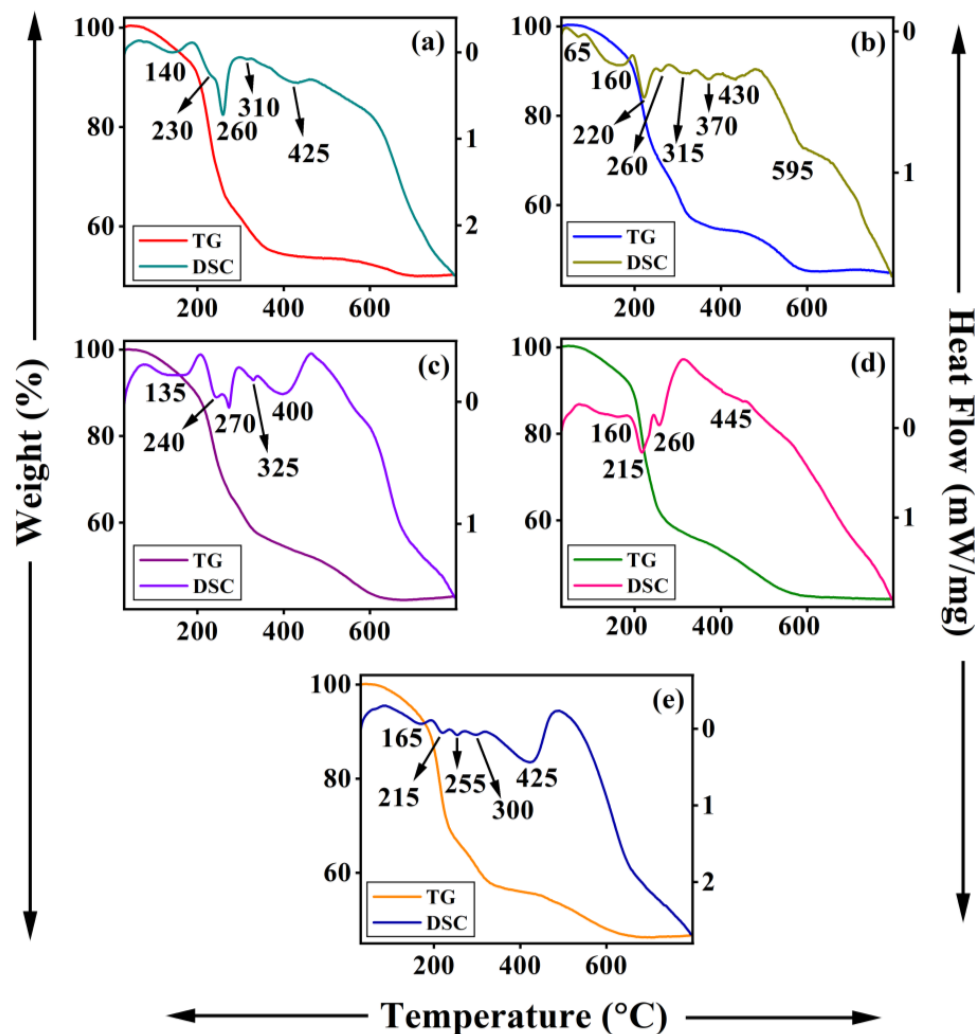


Figure 8. TG-DSC traces of Li-M-Al-DS LDHs where M is (a) Mg, (b) Co, (c) Ni, (d) Cu, and (e) Zn.

Li-Mg-Al-NO₃ LDH demonstrates three weight loss steps in TGA accompanied by three endotherms in DSC measurement consistent with nitrate-intercalated LDH (Figure S3b) [35,36]. Clear changes in TG-DSC traces of Li-M-Al-DS and Li-M-Al-DBS from nitrate-intercalated ternary LDH (Li-Mg-Al-NO₃) substantiate the successful intercalation of DS⁻ and DBS⁻ anions in the interlayer space.

All the samples (Li-M-Al-DS (M = Mg, Co, Ni, Cu, and Zn) LDHs) exhibit characteristic layered morphologies (Figure S5). The morphology of all the divalent metal ion incorporated ternary LDHs differs from the binary Li-Al LDHs. Binary Li-Al LDHs show flaky morphology, while all Li-M-Al-DS LDHs show an agglomeration of plates (Figure S5). Changes in the morphology of ternary LDHs can be related to the incorporation of different divalent metal ions in the LDH framework. EDS analyses of Li-M-Al-DS LDH confirm the presence of divalent metal ions (Mg, Co, Ni, Cu, and Zn) along with Al, C, S, and O in the respective LDH samples (Table S2). All the DS⁻-intercalated Li-M-Al LDH samples exhibit an almost 2:1 ratio of aluminum to divalent metal ions, similar to nitrate-intercalated Li-M-Al LDHs [36], confirming that the divalent metal ions have not been leached out during ion-exchange reactions indicating the stability of the Li-M-Al LDH framework.

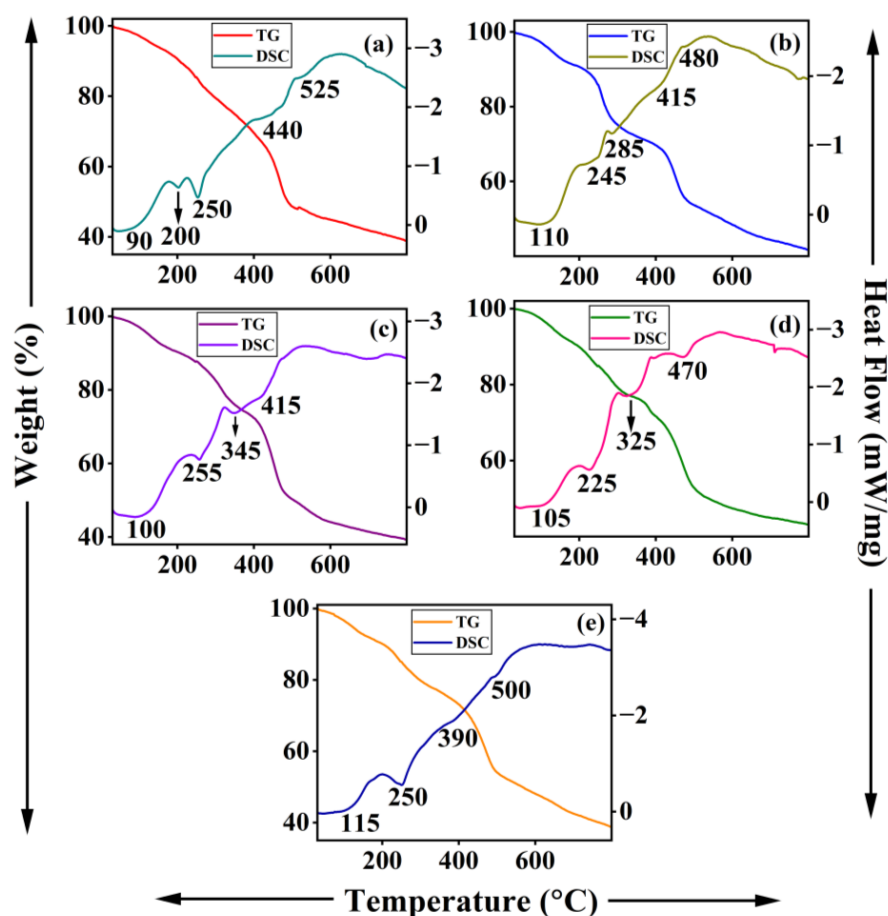


Figure 9. TG-DSC traces of Li-M-Al-DBS LDHs where M is (a) Mg, (b) Co, (c) Ni, (d) Cu, and (e) Zn.

Figure S6 illustrates the SEM images and EDS analyses of Li-M-Al-DBS (M = Mg, Co, Ni, Cu, and Zn) LDHs, in which layered morphology, with aggregates of planar sheets, in contrast to the well-separated plate-like morphology of binary Li-Al-DBS LDH, is noticed. Introducing divalent metal ions in the metal hydroxide layers leads to a change in morphology. The elemental content of Li-M-Al-DBS LDHs is tabulated in Table S2. All the samples show the presence of Al, C, S, and O, along with their corresponding divalent metal ions (Mg, Co, Ni, Cu, and Zn). EDS analyses of surfactant-intercalated ternary LDHs confirm the successful surfactant intercalation in the interlayer region and the divalent metal ion incorporation LDH framework. Moreover, the aluminum to divalent metal ions ratio observed in the corresponding nitrate-intercalated LDH is almost retained, confirming the metal hydroxide layer stability during ion-exchange synthesis. The chemical formula of these surfactant-intercalated Li-M-Al (M = Mg, Co, Ni, Cu, and Zn) LDHs are included in Table 3. In the case of ternary LDHs also, the LDH layer charge is balanced by both CO_3^{2-} and DS^- or DBS^- anions.

3.3. Adsorption of Iodine in Methanol

Li-Al-DBS was closer in its adsorption capacity towards iodine upon examination as it had a higher basal spacing and higher organic content. The iodine adsorption was confirmed by a decrease in the absorbance of characteristic peaks of iodine in methanol centered at 290, 360, and 445 nm (Figure S7).

The effect of contact time on the adsorption of 30 mL (25.4 mg/L) of iodine solution by a 50 mg Li-Al-DBS sample is presented in Figure 10a. The iodine removed in percentage was calculated using

$$R\% = \frac{(C_i - C_t)}{C_i} \times 100 \quad (4)$$

where C_i and C_t are the initial and final iodine concentrations. The iodine removal increases rapidly within 120 min, reaching around 90%. Beyond the time interval of 120 min, the adsorption gets saturated, indicating the establishment of equilibrium. Figure 10b shows the variation of adsorbent dosage on the adsorptive removal of iodine solution (25.4 mg/L). The increased amount of adsorbent leads to the increased adsorption of iodine, and the Li-Al-DBS sample adsorbs nearly 92% of iodine. Any further increase in the amount of the adsorbent does not change the amount of the adsorbed iodine. The adsorption isotherm of iodine solution using a Li-Al-DBS sample as an adsorbent at room temperature is demonstrated in Figure 10c. As the equilibrium concentration of iodine increases, the adsorption capacity of iodine per unit mass of the adsorbent also increases until it reaches equilibrium. The adsorption capacity of the Li-Al-DBS sample for iodine was analyzed by fitting the adsorption isotherm using Langmuir and Freundlich models. The Langmuir and Freundlich models are represented by the following Equations (5) and (6), respectively:

$$\frac{C_e}{q_e} = \frac{C_e}{q_{\max}} + \frac{C_e}{q_{\max}b} \quad (5)$$

$$\ln q_e = \ln K_F + n \ln C_e \quad (6)$$

where C_e (mg/L) is the concentration of the iodine in the solution at adsorption equilibrium, q_e (mg/g) and q_{\max} (mg/g) are the equilibrium and saturated adsorption capacity of the adsorbent per unit mass, respectively, b (L/mg) is the adsorption coefficient of the Langmuir model, K_F is the coefficient of the Freundlich model related to adsorption capacity, and n is the adsorption strength coefficient.

q_{\max} , b , K_F , and n are calculated from the intercept and intercept linear plots (Figures 10d and S8) and compiled in Table 4. According to the parameters fitted by the two adsorption models, the Langmuir model works well, indicating that iodine adsorption on the surface of the Li-Al-DBS sample occurs as monolayers.

Table 4. Characteristic parameters obtained by the Langmuir and Freundlich isotherm models.

q_e (exp)	Langmuir Isotherm Model			Freundlich Isotherm Model		
	q_{\max} (mg/g)	b (L/mg)	R^2	n	K_F (mg/g)	R^2
63.96	67.38	0.16	0.988	0.39	13.64	0.749

The experimental equilibrium adsorption capacity (63.96 mg/g) was close to the theoretical value (67.38 mg/g) obtained according to the Langmuir model.

The adsorption capacity of Li-Al-DBS LDH is compared with other LDHs that have been used as adsorbents for iodine adsorption (Table S3). The Li-Al-DBS LDH exhibits better adsorption capacity than the Mg-Al-NO₃ LDH [54] while there was poor adsorption capacity with respect to Ni-Ti-S_x [44] and Bi-Zn-Al LDH [55]. The possible explanation for the variation in the adsorption capacities could be that the iodine adsorption in the Li-Al-DBS sample takes place via intercalation in addition to other forces while the iodine adsorption in Mg-Al-NO₃-LDH happens mostly by surface adsorption. Ni-Ti-S_x and Bi-Zn-Al-LDHs demonstrate superior adsorption capacities due to chemisorption owing to the presence of S_x²⁻ and Bi³⁺, respectively, along with physisorption [44,55]. S_x²⁻ reduces I₂ to I₃⁻ while Bi³⁺ reduces I₂ to I⁻.

To have better insight into the adsorption process, the experimental data were fitted using the pseudo-first-order (Equation (7)) and pseudo-second-order kinetic equation (Equation (8)). The results are presented in Figure 10e,f and Table 5.

$$\ln(q_e - q_t) = \ln q_e - k_1 t \quad (7)$$

$$\frac{t}{q_t} = \frac{1}{k_2 q_e^2} + \frac{t}{q_e} \quad (8)$$

where q_t and q_e are the adsorption capacities (mg/g) of iodine adsorbed at time t and at equilibrium, respectively. k_1 and k_2 are the equilibrium rate constants for the pseudo-first-order and pseudo-second-order kinetic models, respectively. Figure 10e,f along with Table 5 suggest that the adsorption kinetics of iodine can be better explained by the pseudo-second-order model.

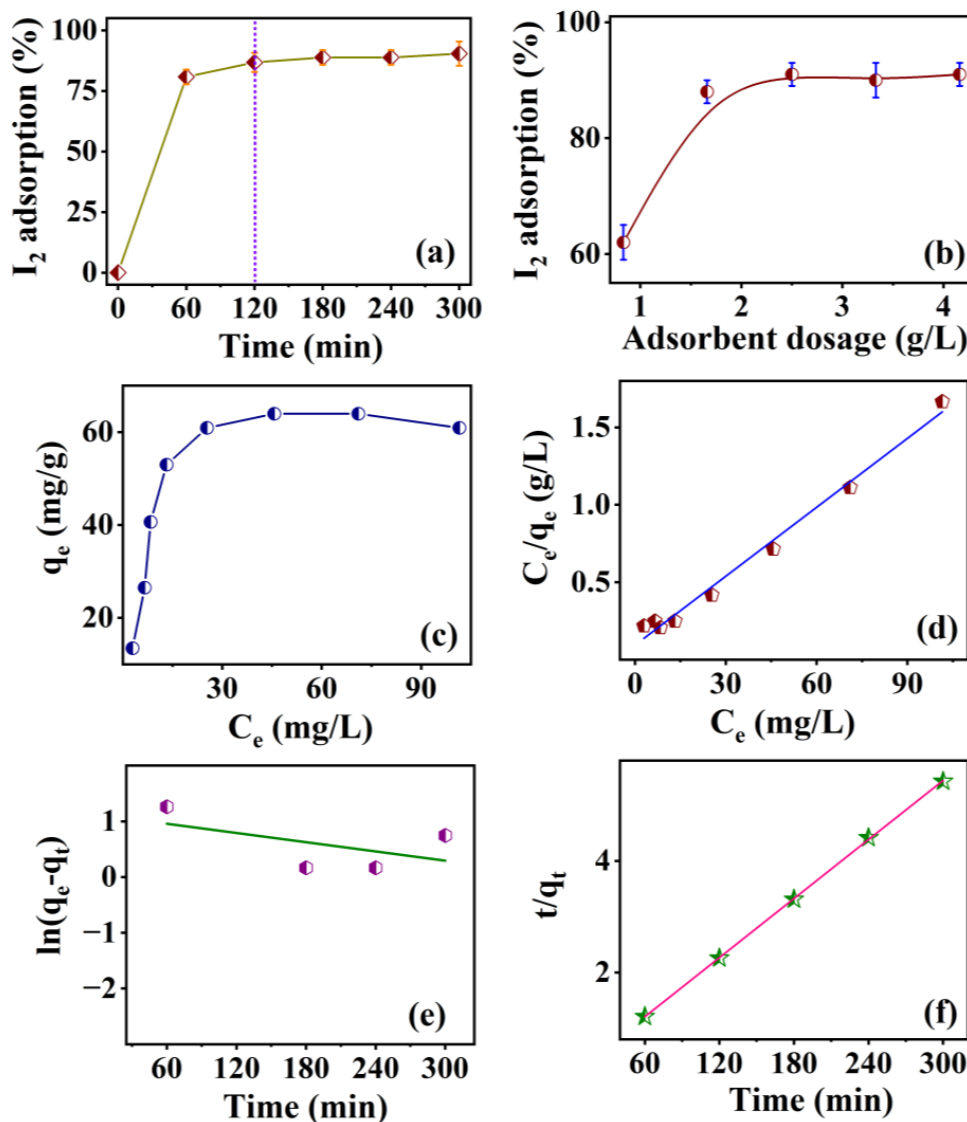


Figure 10. (a) Effect of contact time and (b) effect of adsorbent dosage on percentage of iodine adsorption by Li-Al-DBS sample; (c) adsorption isotherm study; (d) plot of adsorption isotherm data fitted using Langmuir isotherm model; (e) pseudo-first-order kinetics and (f) pseudo-second-order kinetics for iodine adsorption on Li-Al-DBS sample. The dotted line in (a) represents the equilibrium iodine adsorption.

Table 5. The correlated parameters of pseudo-first-order and pseudo-second-order kinetic models for iodine adsorption on Li-Al-DBS sample.

$q_{e,exp}$ (mg/g)	Pseudo-First-Order Model			Pseudo-Second-Order Model		
	k_1 (min^{-1})	$q_{e,cal}$ (mg/g)	R^2	k_2 ($\text{g mg}^{-1} \text{min}^{-1}$)	$q_{e,cal}$ (mg/g)	R^2
53.15	2.76×10^{-3}	3.06	0.713	2.14×10^{-3}	56.59	0.999

The correlation coefficient (R^2) of the pseudo-second-order model is larger and the calculated adsorption capacity ($q_e = 56.59$ mg/g) is closer to the experimental value ($q_e = 53.15$ mg/g). This result suggests that adsorption is a chemical reaction process dominated by rate control rather than simple mass transfer [44,56,57].

4. Conclusions

The surfactant-intercalated binary Li-Al LDHs were successfully synthesized by the ion-exchange reaction assisted by microwaves. The intercalation of dodecyl sulfate and dodecylbenzenesulfonate expanded the basal spacing to ~28 and 30 Å, respectively. ICP-AES and C, H, N, and S microanalyses further substantiated the surfactant-intercalated Li-Al LDHs formation. FTIR spectra confirmed the presence of DS^- and DBS^- anions in Li-Al-DS and Li-Al-DBS LDHs, respectively. DRS and TG-DSC measurements supported the presence of surfactants in the interlayer space. The flaky and plate-like morphology was seen in the SEM images of dodecyl-sulfate- and dodecylbenzenesulfonate-intercalated Li-Al LDH samples, respectively. Surfactant-intercalated ternary Li-M-Al LDHs (M = Mg, Co, Ni, Cu, and Zn) were synthesized by ion exchange from their corresponding nitrate-intercalated LDHs for the first time. PXRD patterns dominated by (00 l) reflections confirmed pure phase formation and successful surfactant intercalation in the interlayer space. ICP-AES and C, H, N, and S analyses confirmed the successful synthesis of surfactant-intercalated ternary LDHs. FTIR and TG-DSC measurements substantiated the presence of surfactants. An agglomerated plate-like morphology was seen in surfactant-intercalated ternary Li-M-Al LDHs compared to binary Li-Al LDHs. The Li-Al-DBS sample showed efficient performance as an adsorbent for removing iodine, confirming the potential applications associated with these surfactant-modified LDH systems.

Supplementary Materials: The following supporting information can be downloaded at: <https://www.mdpi.com/article/10.3390/min13030303/s1>, Figure S1: Diffuse reflectance spectra of Li-Al-DS and Li-Al-DBS LDHs; Figure S2: SEM micrographs and EDS analyses of (a) Li-Al-DS LDH and (b) Li-Al-DBS LDH; Figure S3: (a) FTIR spectrum and (b) TG-DSC traces of Li-Mg-Al-NO₃ LDH; Figure S4: Diffuse reflectance spectra of (a) Li-M-Al-DS and (b) Li-M-Al-DBS (M = Mg, Co, Ni, Cu, and Zn) LDHs; Figure S5: SEM micrographs and EDS analyses of Li-M-Al-DS (M = Mg, Co, Ni, Cu, and Zn) LDH samples; Figure S6: SEM images and EDS analyses of Li-M-Al-DBS (M = Mg, Co, Ni, Cu, and Zn) LDHs; Figure S7: Time-dependent UV-visible spectra of 30 mL (25.4 mg/L) iodine solution in the presence of 50 mg Li-Al-DBS sample; Figure S8: Plot of adsorption isotherm data fitted using Freundlich isotherm model for adsorption of iodine on Li-Al-DBS sample; Table S1: The content of elements in Li-Al-DS, Li-M-Al-DS, Li-Al-DBS, and Li-M-Al-DBS LDHs (M = Mg, Co, Ni, Cu, and Zn) obtained by C, H, N, and S analyses; Table S2: The content of elements in Li-Al-DS, Li-M-Al-DS, Li-Al-DBS, and Li-M-Al-DBS LDHs (M = Mg, Co, Ni, Cu, and Zn) obtained by EDS analyses; Table S3: Iodine adsorption capacity of various LDHs used as adsorbents including the data from the present work.

Author Contributions: Conceptualization, R.N.; methodology, D.K.Y.; validation, D.K.Y.; investigation, D.K.Y.; resources, S.U. and R.N.; data curation, D.K.Y.; writing—original draft preparation, D.K.Y.; writing—review and editing, R.N.; supervision, S.U.; project administration, R.N.; funding acquisition, S.U. and R.N. All authors have read and agreed to the published version of the manuscript.

Funding: The financial support for this work was provided by SERB (CRG/2021/000248), (CRG/2021/003714) Government of India, and the Institute of Eminence Grant (IoE/2021/12/FRP) of University of Delhi.

Data Availability Statement: The data presented in this study are available on request from the corresponding authors.

Acknowledgments: The authors thank the University Science Instrumentation Centre for the use of its facilities. The authors acknowledge the help extended by Vandana Yadav in performing a few experiments. D.K.Y. thanks CSIR for the senior research fellowship.

Conflicts of Interest: The authors declare no conflict of interest.

References

1. Wang, Q.; O'Hare, D. Recent Advances in the synthesis and application of layered double hydroxide (LDH) nanosheets. *Chem. Rev.* **2012**, *112*, 4124–4155. [[CrossRef](#)] [[PubMed](#)]
2. Nalawade, P.; Aware, B.; Kadam, V.J.; Hirlekar, R.S. Layered double hydroxides: A review. *J. Sci. Ind. Res.* **2009**, *68*, 267–272.
3. Williams, G.R.; O'Hare, D. Towards understanding, control and application of layered double hydroxide chemistry. *J. Mater. Chem.* **2006**, *16*, 3065–3074. [[CrossRef](#)]
4. Zhang, F.; Hou, W. Mechano-hydrothermal preparation of Li-Al-OH layered double hydroxides. *Solid State Sci.* **2018**, *79*, 93–98. [[CrossRef](#)]
5. Yu, M.; Li, H.; Du, N.; Hou, W. Understanding Li-Al-CO₃ layered double hydroxides. (I) Urea-supported hydrothermal synthesis. *J. Colloid Interface Sci.* **2019**, *547*, 183–189. [[CrossRef](#)]
6. Thiel, J.P.; Chiang, C.K.; Poeppelmeier, K.R. Structure of lithium aluminum hydroxide dihydrate (LiAl₂(OH)₇·2H₂O). *Chem. Mater.* **1993**, *5*, 297–304. [[CrossRef](#)]
7. Qu, J.; He, X.; Wang, B.; Zhong, L.; Wan, L.; Li, X.; Song, S.X.; Zhang, Q.W. Synthesis of Li-Al layered double hydroxides via a mechanochemical route. *Appl. Clay Sci.* **2016**, *120*, 24–27. [[CrossRef](#)]
8. Lerner, D.W.; Walton, N.R.G. *Contaminated Land, and Groundwater: Future Directions*; The Geological Society: London, UK, 1998; Volume 14, p. 248.
9. Trellu, C.; Mousset, E.; Pechaud, Y.; Huguenot, D.; van Hullebusch, E.D.; Esposito, G.; Oturan, M.A. Removal of hydrophobic organic pollutants from soil washing/flushing solutions: A critical review. *J. Hazard. Mater.* **2016**, *306*, 149–174. [[CrossRef](#)]
10. Van der Oost, R.; Beyer, J.; Vermeulen, N.P. Fish bioaccumulation and biomarkers in environmental risk assessment: A review. *Environ. Toxicol. Pharmacol.* **2003**, *13*, 57–149. [[CrossRef](#)]
11. Pignatello, J.J. Soil organic matter as a nanoporous sorbent of organic pollutants. *Adv. Colloid Interface Sci.* **1998**, *76–77*, 445–467. [[CrossRef](#)]
12. Zhou, W.J.; Wang, X.H.; Chen, C.P.; Zhu, L.Z. Removal of polycyclic aromatic hydrocarbons from surfactant solutions by selective sorption with organo-bentonite. *Chem. Eng. J.* **2013**, *233*, 251–257. [[CrossRef](#)]
13. Ruan, X.X.; Huang, S.; Chen, H.; Qian, G.R. Sorption of aqueous organic contaminants onto dodecyl sulfate intercalated magnesium iron layered double hydroxide. *Appl. Clay Sci.* **2013**, *72*, 96–103. [[CrossRef](#)]
14. Esumi, K.; Yamamoto, S. Adsorption of sodium dodecyl sulfate on hydrotalcite and adsolubilization of 2-naphthol. *Colloids Surf. A Physicochem. Eng. Asp.* **1998**, *137*, 385–388. [[CrossRef](#)]
15. Bruna, F.; Pavlovic, I.; Barriga, C.; Cornejo, J.; Ulibarri, M.A. Adsorption of pesticides carbetamide and metamitron on organohydrotalcite. *Appl. Clay Sci.* **2006**, *33*, 116–124. [[CrossRef](#)]
16. Zhang, M.; Zhao, C.; Li, J.; Xu, L.; Wei, F.; Hou, D.; Sarkar, B.; Ok, Y.S. Organo-layered double hydroxides for the removal of polycyclic aromatic hydrocarbons from soil washing effluents containing high concentrations of surfactants. *J. Hazard. Mater.* **2019**, *373*, 678–686. [[CrossRef](#)]
17. Lee, J.-H.; Zhang, W.; Ryu, H.-J.; Choi, G.; Choi, J.Y.; Choy, J.-H. Enhanced thermal stability and mechanical property of EVA nanocomposites upon addition of organo-intercalated LDH nanoparticles. *Polymer* **2019**, *177*, 274–281. [[CrossRef](#)]
18. Adachi-Pagano, M.; Forano, C.; Besse, J.-P. Delamination of layered double hydroxides by use of surfactants. *Chem. Commun.* **2000**, *2000*, 91–92. [[CrossRef](#)]
19. Leroux, F.; Adachi-Pagano, M.; Intissar, M.; Chauviere, S.; Forano, C.; Besse, J.-P. Delamination and restacking of layered double hydroxides. *J. Mater. Chem.* **2001**, *11*, 105–112. [[CrossRef](#)]
20. O'Leary, S.; O'Hare, D.; Seely, G. Delamination of layered double hydroxides in polar monomers: New LDH-acrylate nanocomposites. *Chem. Commun.* **2002**, *2002*, 1506–1507. [[CrossRef](#)]
21. Hibino, T.; Jones, W. New approach to the delamination of layered double hydroxides. *J. Mater. Chem.* **2001**, *11*, 1321. [[CrossRef](#)]
22. Singh, M.; Ogden, M.I.; Parkinson, G.M.; Buckley, C.E.; Conolly, J. Delamination and re-assembly of surfactant-containing Li/Al layered double hydroxides. *J. Mater. Chem.* **2004**, *14*, 871. [[CrossRef](#)]
23. Hibino, T.; Kobayashi, M. Delamination of layered double hydroxides in water. *J. Mater. Chem.* **2005**, *15*, 653–656. [[CrossRef](#)]
24. Rajamathi, J.T.; Ravishankar, N.; Rajamathi, M. Delamination-restacking behaviour of surfactant intercalated layered hydroxy double salts, M₃Zn₂(OH)₈(surf)₂·2H₂O [M = Ni, Co, and surf = dodecyl sulfate (DS), dodecyl benzene sulfonate (DBS)]. *Solid State Sci.* **2005**, *7*, 195–199. [[CrossRef](#)]
25. Itaya, K.; Chang, H.-C.; Uchida, I. Anion-exchanged clay (hydrotalcite-like compounds) modified electrodes. *Inorg. Chem.* **1987**, *26*, 624–626. [[CrossRef](#)]
26. Qiu, J.; Villemure, G. Anionic clay modified electrodes: Electrochemical activity of nickel (II) sites in layered double hydroxide films. *J. Electroanal. Chem.* **1995**, *395*, 159–166. [[CrossRef](#)]
27. Abend, S.; Bonnke, N.; Gutschner, U.; Lagaly, G. Stabilization of emulsions by heterocoagulation of clay minerals and layered double hydroxides. *Colloid Polym. Sci.* **1998**, *276*, 730–737. [[CrossRef](#)]
28. Lagaly, G.; Mecking, O.; Penner, D. Colloidal magnesium aluminum hydroxide and heterocoagulation with a clay mineral. II. Heterocoagulation with sodium montmorillonite. *Colloid Polym. Sci.* **2001**, *279*, 1097–1103. [[CrossRef](#)]

29. Lagaly, G.; Mecking, O.; Penner, D. Colloidal magnesium aluminum hydroxide and heterocoagulation with a clay mineral. I. Properties of colloidal magnesium aluminum hydroxide. *Colloid Polym. Sci.* **2001**, *279*, 1090–1096. [[CrossRef](#)]
30. Meyn, M.; Beneke, K.; Lagaly, G. Anion-exchange reactions of layered double hydroxides. *Inorg. Chem.* **1990**, *29*, 5201–5207. [[CrossRef](#)]
31. Chen, Z.; Fan, Q.; Huang, M.; Cölfen, H. Synthesis of two-dimensional layered double hydroxides: A systematic overview. *CrystEngComm* **2022**, *24*, 4639–4655. [[CrossRef](#)]
32. Rosa, R.; Leonelli, C.; Villa, C.; Priarone, G. Microwave-assisted melt reaction method for the intercalation of carboxylic acid anions into layered double hydroxides. *J. Microw. Power Electromagn. Energy* **2013**, *47*, 12–23. [[CrossRef](#)]
33. Foruzin, L.J.; Rezvani, Z. Microwave-assisted synthesis of Tartrazine/layered double hydroxide nano-hybrids with high photoluminescent properties: Influence of microwave energy. *Mater. Chem. Phys.* **2021**, *267*, 124716. [[CrossRef](#)]
34. Cosano, D.; Esquivel, D.; Romero, F.J.; Jiménez-Sanchidrián, C.; Ruiz, J.R. Microwave-assisted synthesis of hybrid organo-layered double hydroxides containing cholate and deoxycholate. *Mater. Chem. Phys.* **2019**, *225*, 28–33. [[CrossRef](#)]
35. Pokhriyal, M.; Yadav, D.K.; Pal, S.; Uma, S.; Nagarajan, R. Rapid and one-step transformation of LiAlH₄ to inorganic and organic anion intercalated Li-Al layered double hydroxides. *Eur. J. Inorg. Chem.* **2019**, *2019*, 2412–2418. [[CrossRef](#)]
36. Yadav, D.K.; Uma, S.; Nagarajan, R. Microwave-assisted synthesis of ternary Li-M-Al LDHs (M = Mg, Co, Ni, Cu, Zn, and Cd) and examining their use in phenol oxidation. *Appl. Clay Sci.* **2022**, *228*, 106655. [[CrossRef](#)]
37. He, L.; Liu, S.; Chen, L.; Dai, X.; Li, J.; Zhang, M.; Ma, F.; Zhang, C.; Yang, Z.; Zhou, R.; et al. Mechanism unraveling for ultrafast and selective ⁹⁹TcO₄ uptake by a radiation-resistant cationic covalent organic framework: A combined radiological experiment and molecular dynamics simulation study. *Chem. Sci.* **2019**, *10*, 4293–4305. [[CrossRef](#)]
38. Yu, J.; Luo, X.; Liu, B.; Zhou, J.; Feng, J.; Zhu, W.; Wang, S.; Zhang, Y.; Lin, X.; Chen, P. Bayberry tannin immobilized bovine serum albumin nanospheres: Characterization, irradiation stability and selective removal of uranyl ions from radioactive wastewater. *J. Mater. Chem. A* **2018**, *6*, 15359–15370. [[CrossRef](#)]
39. Li, J.; Dai, X.; Zhu, L.; Xu, C.; Zhang, D.; Silver, M.A.; Li, P.; Chen, L.; Li, Y.; Zuo, D.; et al. ⁹⁹TcO₄ remediation by a cationic polymeric network. *Nat. Commun.* **2018**, *9*, 3007. [[CrossRef](#)]
40. Wu, Y.; Pang, H.; Liu, Y.; Wang, X.; Yu, S.; Fu, D.; Chen, J.; Wang, X. Environmental remediation of heavy metal ions by novel-nanomaterials: A review. *Environ. Pollut.* **2019**, *246*, 608–620. [[CrossRef](#)]
41. Liu, X.; Ma, R.; Wang, X.; Ma, Y.; Yang, Y.; Zhuang, L.; Zhang, S.; Jehan, R.; Chen, J.; Wang, X. Graphene oxide-based materials for efficient removal of heavy metal ions from aqueous solution: A review. *Environ. Pollut.* **2019**, *252*, 62–73. [[CrossRef](#)]
42. Mohanambe, L.; Vasudevan, S. Insertion of iodine in a functionalized inorganic layered solid. *Inorg. Chem.* **2004**, *43*, 6421–6425. [[CrossRef](#)] [[PubMed](#)]
43. Ma, S.; Islam, S.M.; Shim, Y.; Gu, Q.; Wang, P.; Li, H.; Sun, G.; Yang, X.; Kanatzidis, M.G. Highly efficient iodine capture by layered double hydroxides intercalated with polysulfides. *Chem. Mater.* **2014**, *26*, 7114–7123. [[CrossRef](#)]
44. Lin, G.; Zhu, L.; Duan, T.; Zhang, L.; Liu, B.; Lei, J. Efficient capture of iodine by a polysulfide-inserted inorganic NiTi-layered double hydroxides. *Chem. Eng. J.* **2019**, *378*, 122181. [[CrossRef](#)]
45. Wang, D.Y.; Costa, F.R.; Vyalikh, A.; Leuteritz, A.; Scheler, U.; Jehnichen, D.; Wagenknecht, U.; Häußler, L.; Heinrich, G. One-step synthesis of organic LDH and its comparison with regeneration and anion exchange method. *Chem. Mater.* **2009**, *21*, 4490–4497. [[CrossRef](#)]
46. Deng, L.; Zeng, H.; Shi, Z.; Zhang, W.; Luo, J. Sodium dodecyl sulfate intercalated and acrylamide anchored layered double hydroxides: A multifunctional adsorbent for highly efficient removal of Congo red. *J. Colloid Interface Sci.* **2018**, *521*, 172–182. [[CrossRef](#)]
47. He, H.P.; Ray, F.L.; Zhu, J.X. Infrared study of HDTMA⁺ intercalated montmorillonite. *Spectrochim. Acta A* **2004**, *60*, 2853–2859.
48. Bouraada, M.; Ouali, M.S.; de Ménorval, L.C. Dodecylsulfate and dodecyl benzenesulfonate intercalated hydrotalcites as adsorbent materials for the removal of BBR acid dye from aqueous solutions. *J. Saudi Chem. Soc.* **2016**, *20*, 397–404. [[CrossRef](#)]
49. Zhang, F.R.; Du, N.; Song, S.; Hou, W.G. Mechano-hydrothermal synthesis of SDS intercalated LDH nanohybrids and their removal efficiency for 2,4-dichlorophenoxyacetic acid from aqueous solution. *Mater. Chem. Phys.* **2015**, *152*, 95–103. [[CrossRef](#)]
50. Wang, B.; Zhang, H.; Evans, D.; Duan, X. Surface modification of layered double hydroxides and incorporation of hydrophobic organic compounds. *Mater. Chem. Phys.* **2005**, *92*, 190–196. [[CrossRef](#)]
51. Costa, F.R.; Leuteritz, A.; Wagenknecht, U.; Jehnichen, D.; Häußler, L.; Heinrich, G. Intercalation of Mg-Al layered double hydroxide by anionic surfactants: Preparation and characterization. *Appl. Clay Sci.* **2008**, *38*, 153–164. [[CrossRef](#)]
52. Babakhani, S.; Talib, Z.A.; Hussein, M.Z.; Ahmed, A.A.A. Optical and thermal properties of Zn/Al-layered double hydroxide nanocomposite intercalated with sodium dodecyl sulfate. *J. Spectrosc.* **2014**, *2014*, 467064. [[CrossRef](#)]
53. Li, P.G.; Lv, F.Z.; Xu, Z.X.; Qi, G.G.; Zhang, Y.H. Functions of surfactants in the one-step synthesis of surfactant-intercalated LDHs. *J. Mater. Sci.* **2013**, *48*, 5437–5446. [[CrossRef](#)]
54. Kentjono, L.; Liu, J.C.; Chang, W.C.; Irawan, C. Removal of boron and iodine from optoelectronic wastewater using Mg-Al(NO₃) layered double hydroxide. *Desalination* **2010**, *262*, 280–283. [[CrossRef](#)]
55. Dinh, T.D.; Zhang, D.; Tuan, V.N. High iodine adsorption performances under off-gas conditions by bismuth-modified ZnAl-LDH layered double hydroxide. *RSC Adv.* **2020**, *10*, 14360–14367. [[CrossRef](#)]

56. Yao, W.; Wu, Y.; Pang, H.; Wang, X.; Yu, S.; Wang, X. In-Situ reduction synthesis of manganese dioxide@polypyrrole core/shell nanomaterial for highly efficient enrichment of U (VI) and Eu (III). *Sci. China Chem.* **2018**, *61*, 812–823. [[CrossRef](#)]
57. Zhang, C.; Li, X.; Chen, Z.; Tao, W.; Huang, S.; Hayat, T.; Alsaedi, A.; Wang, X. Synthesis of ordered mesoporous carbonaceous materials and their highly efficient capture of uranium from solutions. *Sci. China Chem.* **2018**, *61*, 281–293. [[CrossRef](#)]

Disclaimer/Publisher's Note: The statements, opinions and data contained in all publications are solely those of the individual author(s) and contributor(s) and not of MDPI and/or the editor(s). MDPI and/or the editor(s) disclaim responsibility for any injury to people or property resulting from any ideas, methods, instructions or products referred to in the content.